Verified regularized interval orbit propagation

Geul, Jacco; Mooij, Erwin; Noomen, Ron

DOI
10.2514/1.G004947

Publication date
2021

Document Version
Accepted author manuscript

Published in
Journal of Guidance, Control, and Dynamics

Verified Regularized Interval Orbit Propagation

Jacco Geul[a], Erwin Mooij[b], and Ron Noomen[c]
Delft University of Technology, The Netherlands

Verified interval orbit propagation provides mathematically guaranteed solutions of satellite position and velocity over time. These verified solutions are useful for conjunction analysis and other space-situational-awareness activities. Unfortunately, verified methods suffer from overestimation and explosive interval growth, limiting the possible propagation time and thus their applicability. Different orbital-element state models have been shown to increase the maximum propagation time to a degree, but at the expense of significant overestimation introduced by the state transformations. This paper proposes the Dromo state model for verified integration. Dromo is a regularized variation-of-parameter formulation of the perturbed two-body equations of motion. Taylor models are implemented for both integration and transformation. Moreover, a technique is developed for dealing with time uncertainty resulting from verified regularized propagation. Dromo significantly prolongs the maximum forecasting window, producing verified trajectories of days up to weeks in duration for the low-Earth orbit regime. A sensitivity analysis of the integrator settings identifies combinations that produce stable and computationally efficient solutions. A sensitivity study of the orbital parameters shows that the method is applicable to a large orbital regime, especially for low-Earth orbit regions that contain high densities of space debris.

[a] Ph.D. Candidate, Section Astrodynamics and Space Missions, Faculty of Aerospace Engineerin ; j.geul@tudelft.nl.
[b] Assistant Professor, Section Astrodynamics and Space Missions, Faculty of Aerospace Engineerin ; e.mooij@tudelft.nl. Associate Fellow AIAA.
[c] Assistant Professor, Section Astrodynamics and Space Missions, Faculty of Aerospace Engineerin ; r.noomen@tudelft.nl.

I. Introduction

Space debris composes the largest group of observable objects in Earth orbit, and presents a major threat to operational spaceflight [1]. Collision prediction methods generally compute potential collisions, by propagating initial states and state errors as probability density functions to an estimated time of closest approach [2–5]. Verified interval orbit propagation (VIOP) presents a different approach to conjunction analysis [6]. VIOP generates bounds on the state that are guaranteed to encompass the exact solution at any given time. The non-intersection of VIOP solutions mathematically rules out possible collisions, whereas an intersection implies the possibility of a collision, however, with an unknown likelihood. This unique mathematical property makes VIOP interesting for many space-situational-awareness (SSA) activities, potentially in combination with statistical methods. Verified integration has previously been applied to computing Solar-System dynamics [7], intersections between near-Earth objects and Earth [8, 9], and satellite conjunctions [6, 10]. Verified predictions of the Iridium-Cosmos collision were studied in Ref. [6]. The error build-up of regularized formulations was analysed using interval arithmetic in Ref. [11].

Verified methods are known to suffer from overestimation, which results in rapid growth and explosion of the verified solutions after short periods of integration. Different state models are shown to improve the forecasting window up to four to ten times [6]. A differential algebra formulation of the simplified general perturbation (SGP4) model was used for uncertainty propagation in Ref. [12]. Due to the interval transformations from Cartesian coordinates to the propagation state model and back, a large amount of additional overestimation is introduced. Especially, the overestimation resulting from the transformation of the initial uncertainty is included in the propagation, reducing the overall effectiveness. Regularized methods for verified propagation have recently been suggested as a state model [11]. However, the time transformation in regularization brings forth additional practical challenges [13].

This paper aims to increase the time until solution explosion by proposing the regularized Dromo formulation as the state model [14]. Moreover, the research aims to reduce the overestimation in the interval state transformations. Also, the paper proposes a new technique for converting time uncertainty into additional post-propagation uncertainty in position and velocity. The study

primarily focusses on low-Earth orbit (LEO) satellites. LEO presents a demanding environment and is very relevant for collision prediction and avoidance.

The paper is structured as follows. First, a background of interval analysis and verified orbit propagation is provided in Sec. II. Regularized propagation and the proposed Dromo state model are given in Sec. III. The interval state transformations and the developed time uncertainty transformation technique are presented in Sec. IV. In Sec. V, the models and set-up of the study are explained. Section VI shows the results of the transformation techniques, a comparison of Dromo with other state models, and a sensitivity analysis into the integrator settings and orbital parameters. Lastly, the conclusions are given in Sec. VII.

II. Verified Propagation

VIOP is an uncertainty analysis method that applies initial-value-problem (IVP) interval methods to the satellite equations of motion (EOMs). In this, the initial uncertainty, model uncertainty, and numerical truncation and rounding errors are modeled and bound by intervals. VIOP provides a verified interval solution of the position and velocity of a satellite trajectory over time, which is mathematically guaranteed to contain all possible trajectories. This characteristic makes verified integration interesting for many different applications.

A classical application of VIOP in celestial mechanics is the propagation of asteroid state vectors [7, 15]. If the interval solution, which encloses all possible trajectories, fails to intersect the Earth, an impact can be mathematically ruled out. This is opposed to statistical methods, which only ascribe probabilities to certain events, and are not able to rule any out

It is realistic to consider that for physical applications, the mathematical proof holds for the model (i.e., the ordinary differential equations (ODEs) and its parameters) and the given initial conditions. Inherently, the mathematical model has a limited fidelity and the initial conditions are often not known perfectly (e.g., derived from observations). So the mathematically guaranteed solution does not necessarily translate to the physical world. To account for this, the modeling and initial condition errors have to be conservatively estimated and included in the uncertainty of the system.

Interval analysis (IA) in general and Taylor Models (TM) specifically are presented in Sec. II.A.

IA suffers from overestimation, which is the inclusion of trajectories that should not be contained within the interval. Several sources of overestimation are discussed in detail in Sec. II.B. Finally, Sec. II.C discusses the verified solution of initial value problems.

A. Interval Analysis and Taylor Models

IA is an extension of real-number arithmetic to intervals and was developed by Moore in the early 1960s [16]. A real interval X is defined as the set of real numbers lying within (and including) a given lower and upper bound:

$$X = [\underline{X}, \overline{X}] = \{x \in \mathbb{R} \,|\, \underline{X} \leq x \leq \overline{X}\} \tag{1}$$

where the under- and overline indicate the lower and upper bound, respectively. The width of the interval is calculated as $w(X) = \overline{X} - \underline{X}$, and the midpoint as $m(X) = (\underline{X} + \overline{X})/2$. IA describes rules for the basic arithmetic operations, such as addition, multiplication, and inversion [17]:

$$X + Y = [\underline{X} + \underline{Y}, \overline{X} + \overline{Y}] \tag{2}$$

$$XY = [\min(\underline{X}\underline{Y}, \underline{X}\overline{Y}, \overline{X}\underline{Y}, \overline{X}\overline{Y}), \max(\underline{X}\underline{Y}, \underline{X}\overline{Y}, \overline{X}\underline{Y}, \overline{X}\overline{Y})] \tag{3}$$

$$X^{-1} = [\overline{X}^{-1}, \underline{X}^{-1}] \tag{4}$$

where a special formulation of the inversion is used when $0 \in X$.

Most mathematical operations and functions have been defined for IA, as well as expansion to interval vectors and matrices. An example of an interval calculation is presented in Sec. II.B.2. When interval calculations are performed numerically, special rounding techniques ensure that the interval bounds are always rounded outward to the next machine-representable number. This ensures that rounding errors are absorbed within the intervals during all computations.

TM recursively computes high-order multivariate polynomial function approximations of IA to reduce overestimation due to the dependency problem. With TM possible cancellation of sub-parts of the function can be detected [18]. The dependency problem is discussed in Section II.B.2. TMs have been developed by Berz and Makino, and Hoefkens since 1996 [15, 18, 19]. The remainder

term rigorously bounds the approximation error, to control the dependency problem of IA [19]. The TM T_f of a function f of up to order k is written as:

$$f(x) \in T_f(x) = p_f(x) + R_f(x) \qquad \text{for } x \in [\underline{X}, \overline{X}] \tag{5}$$

$$p_f(x) = \sum_{n=0}^{k} \frac{f^{(n)}(a)}{n!}(x-a)^n \tag{6}$$

where $p_f(x)$ is the expansion of $f(x)$ around a up to order k. The interval remainder is R_f. To obtain the interval remainder bound, the remainder, i.e., the $(k+1)$th term, of the series expansion can be quantitatively bounded using different interval methods. The choice of method has a significant impact on the performance of TMs and many bounding schemes have been proposed [20, 21].

B. Overestimation

Overestimation is the inclusion of non-solutions within the interval. Three sources for overestimation can be distinguished: wrapping, cancellation, and dependency. Wrapping and dependency are discussed in more detail below. Cancellation occurs when the regular floating-point result of an operation has a small magnitude compared to the individual numbers, for instance, when subtracting two large and nearly equal numbers. The floating-point result is a number of relatively small magnitude, while in IA the widths of the interval are always additive and thus result in a large interval with large overestimation [20].

In recurrent computations, overestimation leads to the inclusion of non-solutions in subsequent analyses, giving rise to even more overestimation. This leads to a phenomenon known as interval explosion: an exponential growth of the interval solution. When interval explosion occurs, further computation becomes physically nonsensical. Interval explosion can also occur for stable dynamical systems.

1. Wrapping

Wrapping occurs when the true shape of the uncertainty cannot be sufficiently represented by an interval. Consider an initial uncertainty that is described by a circle. The representation of this uncertainty in Cartesian coordinates results in a square interval. Therefore, the interval contains

many non-solutions outside the original circle. In VIOP, the wrapping effect occurs not only when enclosing the initial uncertainty in interval form, but also at every step of the integration, as the continuous dynamical system is numerically discretized [20]. The recurrent wrapping at each time step might only produce a small amount of overestimation, but cumulatively it can lead to interval explosion.

The wrapping effect can be reduced by choosing a different coordinate system. In the example of the 2D circular uncertainty, polar coordinates can be used to perfectly describe the uncertainty without any overestimation at all. Likewise, for orbit propagation, different state models can be used to better describe the uncertainty and thus limit wrapping overestimation at each step. Furthermore, state models with slow-varying elements can reduce the number of integration steps necessary and thus the number of times wrapping occurs. The downside of a different state model is that the initial uncertainty and final solution after propagation often need to be transformed, which itself introduces overestimation.

The unified state model (USM) and modified equinoctial elements (MEE) are investigated in Ref. [6], and outperform the classic Cartesian state model significantly in propagation time to solution explosion. The hybrid-interval trajectory is a novel technique proposed in Ref. [6], and propagates multiple state models concurrently. In this approach, only the intersection of the interval solutions (in Cartesian coordinates) becomes the true verified solution. Solutions outside the intersection of the intervals produce overestimation, as verified methods demand that all solutions are enclosed. The technique is effective in reducing the overestimation of the instantaneous verified solution. However, the intersection of the intervals must be computed in a common coordinate system, which introduces overestimation in the transformation. Therefore, hybrid intervals do not improve the propagation time until solution explosion.

2. Dependency Problem

Dependency results from multiple occurrences of one or several variables in a system of equations. While a variable may take on any value within its interval, it must take on the same value in each occurrence. However, this dependency is not taken into account in interval arithmetic [22, 23].

To illustrate the dependency problem, the interval solutions G and H of equivalent functions $g(x)$ and $h(x)$ are computed for $X = [2,\ 3]$ [23]:

$$
\begin{aligned}
g(x) &= \frac{x}{x-1} \\
G([2,\ 3]) &= \frac{[2,\ 3]}{[2,\ 3]-1} = \frac{[2,\ 3]}{[1,\ 2]} = [1,\ 3] \\
h(x) &= 1 + \frac{1}{x-1} \\
H([2,\ 3]) &= 1 + \frac{1}{[2,\ 3]-1} = 1 + \frac{1}{[1,\ 2]} = 1 + [0.5,\ 1] = [1.5,\ 2]
\end{aligned}
$$

where $w(G) = 2$ and $w(H) = 0.5$. G overestimates the true width by a factor four. The dependency problem increases with the complexity of the equations and the number of occurrences. Often, it is not possible to rewrite the equations to reduce dependency.

C. Verified Initial Value Problem Solvers

In traditional IA the solution at each integration step is computed in two stages [24]. In the first stage, the existence and uniqueness of a solution are proven by computing a rough enclosure of the solution, referred to as the *a-priori* solution, which is valid over the integration step, from t_1 to $t_1 + \Delta t$. In the second stage, a tighter solution is computed, which provides the instantaneous verified solution at time t_1. The exact details of each step depend on the specific solver that is used and are not important for the application. The a-priori solutions are used when a continuous solution is desired, while the tight solutions are the starting point for each integration step.

Many software packages exist that use TM for verified integration, including COSY [18], VNODE-LP [22], VSPODE [23], and RiOT [25]. These packages differ in how range bounding is implemented and what techniques are used for computing the tighter enclosure in the second stage. The packages further differ in their availability [26]. A survey of available packages on the basis of propagation time until solution explosion shows that VSPODE (Validating Solver for Parametric ODEs) is very promising [6].

VSPODE uses a unique algorithm for computing tighter enclosures, which addresses the wrapping effect by propagating the intermediate results using TMs as a function of the model parameters and initial values [23]. This means that intervals of both initial state and model parameters are

parametrically expressed in the solution and evaluated in the last step. VSPODE solves parametric autonomous IVPs. For non-autonomous systems, the EOMs need to be adapted to an autonomous form by introducing an additional pseudo-state variable.

The VSPODE solver is controlled by three tuning parameters: k, q, and ϵ, where k is the order of the interval Taylor series (ITS) with respect to time, q is the order of the TM as a function of the initial intervals and uncertain parameters, and ϵ the numerical tolerance controlling the step-size. The order q determines how well the intervals are described as a function of the initial intervals and uncertain parameters, and thus the effectivenes in reducing overestimation when computing tighter enclosures. The sensitivity of the verified solution to the tuning parameters is investigated in Sec. VI.F. Another important parameter of VSPODE is the number of uncertain quantities N_u, which is the sum of uncertain state variables and system parameters. The computational cost of VSPODE is proportional to a power $N_u q$ [23]. Therefore, it is important to minimize N_u, which will be discussed in Secs. V and VI.F.

III. Regularized Propagation

Regularization aims to remove singularities and dynamical instability from the EOMs, leading to less integration errors and more efficient integration. This is achieved by a transformation of the independent variable (in orbital mechanics a Sundman transformation is commonly used for this) and the introduction of a new set of variables instead of position and velocity to represent the motion [27]. Sometimes, these new variables are integrals of the two-body problem, and their variations when the motion is perturbed can be obtained by the variation-of-parameters (VOP) technique, starting from the unperturbed solution of the equations of motion.

A. Dromo and Comparison of Regularized Methods

Two popular methods are Kustaanheimo-Stiefel (KS) [28] and Sperling-Burdet (SB) [29] regularizations. Recently, new special perturbation methods that take advantage of quaternions have been developed [14, 30–36].

Dromo is a modern VOP method derived from the Burdet-Ferrándiz regularization [34, 37]. It has been applied to the propagation of asteroid orbits for computing planetary close encounters,

and for the lifetime analysis of space debris [38]. Dromo is also used for covariance propagation of asteroids [39]. Dromo employs only eight EOMs, which is close to non-regularized methods (often six) and less than other regularized methods: KS and SB feature 10 and 12 differential equations, respectively [40]. In Ref. [14] a new version of Dromo is presented, which allows a separate treatment of perturbing forces that are derivable from a potential and those that are not. The behavior of the EOMs can be further improved through the use of time elements [36].

Dromo is compared against a number of classical and modern methods in Table 1. Stiefel-Scheifele (SS) [41] represents the benchmark for this problem. The table gives the final state of a satellite in a highly eccentric ($e = 0.95$ and $r_p = 6800\,\mathrm{km}$) orbit about the Earth. The motion is perturbed by the Earth's oblateness (J_2) and third-body gravitational attraction of the Moon. The orbit is integrated for 288.127 689 41 mean solar days (roughly 50 revolutions). The final position (R_x, R_y, R_z), number of steps per revolution (steps/rev), and the absolute error with respect to the benchmark are reported. Additional results for Cowell, Dromo, and MEE [13], and USM [42] are added to the original comparison table reported in [43].

On the test problem, all regularized methods (SB, KS and Dromo) perform much better in terms of accuracy than the others. This is not at all surprising as the orbit is highly eccentric. Cowell, MEE and USM are integrated using Runge-Kutta Dormand-Prince 5(4) variable step-size integrator. The final errors of these three methods were matched to the Cowell-E final error by changing the numerical tolerances, to provide a direct comparison of the number of integration steps per revolution. Dromo is only slightly more expensive than KS on this problem, and it performs much better than the other methods on problems with lower eccentricities ($e = 0$, 0.3, 0.7) [13, 36]. The Dromo transformation equations to Cartesian coordinates are more accurate than KS [11]. MEE and USM have much better performance (approaching the performance of Dromo) for less eccentric orbits ($e < 0.3$) [13, 42]. The lean formulation, regularized properties, and good performance on a wide range of problems, make Dromo interesting for verified propagation.

B. Dromo Formulation

In Dromo, the motion is represented by the non-dimensional physical time (ζ_0) and seven parameters, which are first integrals of the two-body problem. Three of the parameters (ζ_{1-3}) fix

Table 1 Comparison of results from literature of several methods for the oblate Earth plus Moon after 288.12768941 days [13, 42, 43].

	SS [43]	SB [43]	KS [43]	Cowell-E[a] [43]
R_x [km]	−24 219.050	−24 218.818	−24 219.002	−24 182.152
R_y [km]	227 962.106	227 961.915	227 962.429	227 943.989
R_z [km]	129 753.442	129 753.343	129 753.822	129 744.270
Steps/rev	500	62	62	240
Error [km]	*baseline*	0.318	0.501	42.5

	Dromo [13]	Cowell[a] [13]	MEE [13]	USM [42]
R_x [km]	−24 218.829	−24 256.391	−24 256.980	−24 219.049
R_y [km]	227 961.980	227 980.068	227 979.117	227 962.106
R_z [km]	129 753.414	129 762.509	129 761.798	129 753.442
Steps/rev	113	453	188	372
Error [km]	0.256	42.4	42.4	42.1

[a] "Cowell-E" indicates the formulation in Ref. [44], which uses the total energy as an independent parameter, while "Cowell" indicates the classic Cartesian formulation.

the shape of the osculating conic and the remaining four are the components of a unit quaternion (ζ_{4-7}), which describes the orientation of the orbital plane and of a reference direction on it. All quantities in Dromo are made non-dimensional by introducing units for time and length as n_0^{-1} and R_0, respectively. These quantities are defined when the Dromo state is first computed. Here, R_0 is the initial radius and n_0 the initial circular mean motion (i.e., $n_0 = n(a{=}R_0) = \sqrt{\mu/R_0^3}$) [14]. For intervals, R_0 is defined as $R_0 = \sqrt{m(X_0)^2 + m(Y_0)^2 + m(Z_0)^2}$. Here $m(X_0)$ is the midpoint of initial interval X_0 in x-direction, as discussed in Section II.A.

The perturbations are expressed in the orbital reference frame (i.e., consisting of the radial, transverse, and normal components [45]) and separated into those derivable and non-derivable from a potential. The separation allows for conservation of energy, when only conservative forces are applied. The total perturbing acceleration $\mathbf{f}$ is given by:

$$\mathbf{f} = \mathbf{P} + \nabla\mathcal{U} \tag{7}$$

where $\mathbf{P}$ is the sum of all perturbations that are non-derivable from a potential and $\nabla\mathcal{U}$ is the gradient of the total perturbing potential.

1. *Equations of Motion*

The physical time t is non-dimensionalized as $\zeta_0 = tn_0$, and is a function of the fictitious time ϕ through Eq. (8). Along Keplerian motion ϕ behaves like the true anomaly. The entire derivation of the elements is presented in Ref. [14], and only the ODEs and relevant transformation equations are presented here. The ODEs of the elements with respect to the independent parameter are [14]

$$\frac{\mathrm{d}\zeta_0}{\mathrm{d}\phi} = \frac{1}{\zeta_3 V_s^2} \tag{8}$$

$$\frac{\mathrm{d}\zeta_1}{\mathrm{d}\phi} = \frac{\sin\phi}{V_s}\left(\frac{f_r}{\zeta_3 V_s} - 2\mathcal{U}\right) - \left(\frac{V_s}{\zeta_3} + 1\right)\cos\phi\frac{\mathrm{d}\zeta_3}{\mathrm{d}\phi} \tag{9}$$

$$\frac{\mathrm{d}\zeta_2}{\mathrm{d}\phi} = \frac{\cos\phi}{V_s}\left(2\mathcal{U} - \frac{f_r}{\zeta_3 V_s}\right) - \left(\frac{V_s}{\zeta_3} + 1\right)\sin\phi\frac{\mathrm{d}\zeta_3}{\mathrm{d}\phi} \tag{10}$$

$$\frac{\mathrm{d}\zeta_3}{\mathrm{d}\phi} = -\frac{1}{V_s^4}\left[\zeta_3 V_r V_s\left(2\mathcal{U} - \frac{\zeta_3 V_s}{V_s + \zeta_3}\frac{\partial\mathcal{U}}{\partial\zeta_3}\right) + V_t P_t + \frac{\partial\mathcal{U}}{\partial t}\right] \tag{11}$$

$$\frac{\mathrm{d}\zeta_4}{\mathrm{d}\phi} = \frac{1}{2V_s}\left[\frac{f_n}{\zeta_3 V_s V_t}(\zeta_7\cos\Delta\phi - \zeta_6\sin\Delta\phi) + \zeta_5(V_t - V_s)\right] \tag{12}$$

$$\frac{\mathrm{d}\zeta_5}{\mathrm{d}\phi} = \frac{1}{2V_s}\left[\frac{f_n}{\zeta_3 V_s V_t}(\zeta_6\cos\Delta\phi + \zeta_7\sin\Delta\phi) - \zeta_4(V_t - V_s)\right] \tag{13}$$

$$\frac{\mathrm{d}\zeta_6}{\mathrm{d}\phi} = -\frac{1}{2V_s}\left[\frac{f_n}{\zeta_3 V_s V_t}(\zeta_5\cos\Delta\phi - \zeta_4\sin\Delta\phi) - \zeta_7(V_t - V_s)\right] \tag{14}$$

$$\frac{\mathrm{d}\zeta_7}{\mathrm{d}\phi} = -\frac{1}{2V_s}\left[\frac{f_n}{\zeta_3 V_s V_t}(\zeta_4\cos\Delta\phi + \zeta_5\sin\Delta\phi) + \zeta_6(V_t - V_s)\right] \tag{15}$$

where f_r and f_n are the radial and normal components of the total perturbing acceleration vector and P_t the transverse component of all perturbing accelerations not derived from a potential. The

pseudo-transverse V_s, transverse V_t, and radial velocity V_r are given by

$$V_s = \zeta_3 + \zeta_1 \cos\phi + \zeta_2 \sin\phi \tag{16}$$

$$V_t = \sqrt{V_s^2 - 2\mathcal{U}} \tag{17}$$

$$V_r = \zeta_1 \sin\phi - \zeta_2 \cos\phi \tag{18}$$

It is important to note that $\Delta\phi$ in Eqs. (12)-(15) represents the difference between the current and initial value of the independent variable ($\Delta\phi = \phi - \phi_0$), and not the step size. The initial value of ϕ_0 can be arbitrarily chosen when the initial Dromo state is constructed. A common choice for ϕ_0 is the initial true anomaly $\phi_0 = \nu_0$ or just $\phi_0 = 0$.

Alternatively, when the contribution of the perturbation ($\mathbf{P}$) to the total perturbation ($\mathbf{f}$) is small, the ODE of the third element ζ_3 can be replaced by that of the total specific energy $\mathcal{E}$:

$$\frac{\mathrm{d}\mathcal{E}}{\mathrm{d}\phi} = \frac{1}{\zeta_3 V_s^2}\left(V_r P_r + P_t\sqrt{V_s^2 - 2\mathcal{U}} + \frac{\partial \mathcal{U}}{\partial t}\right) \tag{19}$$

where ζ_3 can then be obtained through the following equation [14]:

$$\zeta_3 = \sqrt{\zeta_1^2 + \zeta_2^2 - 2\mathcal{E}} \tag{20}$$

2. From Dromo to Cartesian Coordinates

Cartesian coordinates are directly obtained through the transformation matrix $\mathbf{C}_{\mathcal{RI}}$ of the local-vertical local-horizontal frame $\mathcal{R}$ to the inertial frame $\mathcal{I}$, defined by [14]:

$$\mathbf{C}_{\mathcal{RI}} = \mathbf{C}_0 \mathbf{C}_\phi \tag{21}$$

$$\mathbf{C}_0 = \begin{bmatrix} 1-2\zeta_5^2-2\zeta_6^2 & 2\zeta_4\zeta_5-2\zeta_6\zeta_7 & 2\zeta_4\zeta_6+2\zeta_5\zeta_7 \\ 2\zeta_4\zeta_5+2\zeta_6\zeta_7 & 1-2\zeta_4^2-2\zeta_6^2 & 2\zeta_5\zeta_6-2\zeta_4\zeta_7 \\ 2\zeta_4\zeta_6-2\zeta_5\zeta_7 & 2\zeta_5\zeta_6+2\zeta_4\zeta_7 & 1-2\zeta_4^2-2\zeta_5^2 \end{bmatrix} \tag{22}$$

$$\mathbf{C}_\phi = \begin{bmatrix} \cos\Delta\phi & -\sin\Delta\phi & 0 \\ \sin\Delta\phi & \cos\Delta\phi & 0 \\ 0 & 0 & 1 \end{bmatrix} \tag{23}$$

The non-dimensional Cartesian position and velocity components are obtained as:

$$[R_X,\, R_Y,\, R_Z]^\intercal = \mathbf{C}_{\mathcal{RI}}[r,\, 0,\, 0]^\intercal \tag{24}$$

$$[V_X,\, V_Y,\, V_Z]^\intercal = \mathbf{C}_{\mathcal{RI}}[V_r,\, V_t,\, 0]^\intercal \tag{25}$$

where the position and velocity can be dimensionalized using the quantities R_0 and n_0, for distance and time, respectively, as defined previously.

3. From Cartesian to Dromo Elements

Before transformation, the Cartesian coordinates are first non-dimensionalized using the quantities R_0 and n_0, as described in Sec. III.B. The orbital radius r, radial velocity V_r, transverse velocity V_t, and pseudo-transverse velocity V_s are first calculated using [14]:

$$r = \sqrt{R_X^2 + R_Y^2 + R_Z^2} \tag{26}$$

$$h = \|\mathbf{h}\| = \|\mathbf{r} \times \mathbf{v}\| \tag{27}$$

$$V_r = \frac{\mathbf{r} \cdot \mathbf{v}}{r} \tag{28}$$

$$V_t = \frac{h}{r} \tag{29}$$

$$V_s = \sqrt{V_t^2 + 2\mathcal{U}} \tag{30}$$

which are used to express the Dromo parameters ζ_{1-3}, and the transformation matrices $\mathbf{C}_{\mathcal{RI}}$ and $\mathbf{C}_0$:

$$\zeta_3 = \frac{1}{rV_s} \tag{31}$$

$$\zeta_1 = (V_s - \zeta_3)\cos\phi_0 + V_r \sin\phi_0 \tag{32}$$

$$\zeta_2 = (V_s - \zeta_3)\sin\phi_0 - V_r \cos\phi_0 \tag{33}$$

$$\mathbf{C}_{\mathcal{RI}} = \left(\frac{\mathbf{r}}{r},\ \frac{\mathbf{h}}{h} \times \frac{\mathbf{r}}{r},\ \frac{\mathbf{h}}{h}\right) \tag{34}$$

$$\mathbf{C}_0 = \mathbf{C}_{\mathcal{RI}}\mathbf{C}_\phi^\intercal \tag{35}$$

The quantity ζ_0 is simply the non-dimensionalized physical time. The initial value of t can be chosen arbitrarily, and in this study it is always set equal to 0. Note that $\zeta_3 \to \infty$ as $rV_s \to 0$, however, it can be assumed that this is not realized for the considered motion in the presence of a non-zero potential(see Eq.(30)) and radius $r >> 0$. The remaining elements can be found by using the transformation matrix $\mathbf{C}_0$:

$$\zeta_7 = \frac{1}{2}\sqrt{1 + \mathbf{C}_0(1,\,1) + \mathbf{C}_0(2,\,2) + \mathbf{C}_0(3,\,3)} \tag{36}$$

$$\zeta_4 = \frac{\mathbf{C}_0(3,\,2) - \mathbf{C}_0(2,\,3)}{4\zeta_7} \tag{37}$$

$$\zeta_5 = \frac{\mathbf{C}_0(1,\,3) - \mathbf{C}_0(3,\,1)}{4\zeta_7} \tag{38}$$

$$\zeta_6 = \frac{\mathbf{C}_0(2,\,1) - \mathbf{C}_0(1,\,2)}{4\zeta_7} \tag{39}$$

where $\mathbf{C}_0(i,j)$ denotes the element of $\mathbf{C}_0$ in the i-th row and j-th column. When $\zeta_7 = 0$ special formulas for the elements ζ_{4-6} have to be used, which can be found in Ref. [14].

IV. Methodology

Dromo is proposed as a state model to further improve the propagation time to solution explosion. The use of a regularized formulation is here referred to as verified regularized interval orbit propagation (VRIOP). Cartesian coordinates are used to express the initial state and uncertainty and perform analysis after propagation, such as computing conjunctions. All initial uncertainties

are assumed to be represented by intervals.

The simplest uncertainty transformation method is Monte Carlo (MC), where the uncertainty distribution (in this case an interval) is sampled to a sufficient degree and each individual sample is transformed to the propagation state model, to construct the new transformed distribution. For interval transformation, the minimum and maximum values in each dimension are taken to be the new intervals. MC intervals are non-verified as the obtained intervals only approach the true interval. Verified interval transformation techniques will be discussed in Sec. IV.A.

The physical time has become a dependent variable and thus has an uncertainty that will grow with propagation. The uncertainty in the time variable needs to be converted to additional position and velocity uncertainty. A new procedure for this is proposed in Sec. IV.B.

A. Verified Transformations

Verified transformation ensures that solution enclosure is maintained. Any IA technique can be used for the transformation and does not have to match the technique used for the propagation. For example, IA is used for the transformations and TM for the propagation in Ref. [6].

Transformations give rise to additional overestimation due to the non-linear equations. Also the transformation needs to be performed twice: once to the propagation state model and once more after integration, back to Cartesian coordinates. The overestimation introduced by the transformation results in a large additional uncertainty even before any propagation is done and can even outweigh the benefits an alternative state model may provide. In Ref. [6] the MEE and USM are compared against Cartesian coordinates for the VIOP of a LEO satellite. The different solutions explode after a different time of propagation. To illustrate the effects of the transformations and the benefits of different propagation models, the results have been reproduced in Fig. 1. The results for Dromo will be directly compared to the same trial in Sec. VI.D.

Due to the additional uncertainty from the transformations, the Cartesian solution outperforms the MEE and USM until a propagation time of 4 h. The initial volumes of MEE and USM transformed back to Cartesian coordinates are 703 and 601 km^3, respectively. Considering that the initial uncertainty is only $1 \times 10^{-6}\,\mathrm{km}^3$, the overestimation due to transformation is very large indeed.

Figure 1 shows once and twice-per-orbit oscillations of the volumes. For Cartesian coordinates

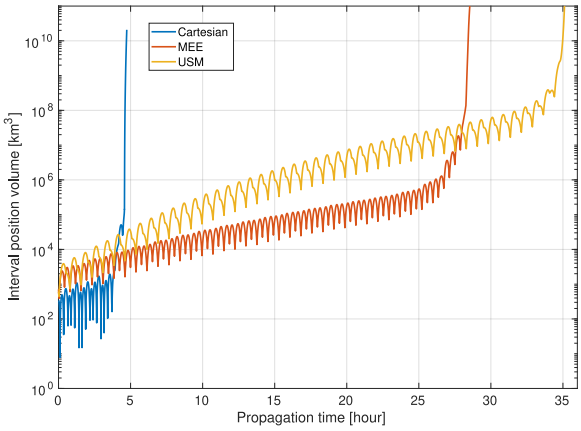

Fig. 1 Position interval volume growth with propagation time for the Cartesian, MEE, and USM state models (reproduced from Fig.7 of Ref. [6]).

the oscillation is by far the largest. These oscillations illustrate the overestimation due to wrapping in a Cartesian cuboid as the uncertainty is rotated along a full orbit.

IA transformations are shown to a produce large overestimation for MEE and USM [6]. IA and TM transformations are implemented in this research. TM transformations follow the same two-step approach as TM integration: a rough solution enclosure is first computed, which is then tightened using TM. The TM is expressed as a function of the original Cartesian initial interval conditions. Dependency arising from the transformation equations can be reduced when the tighter solution is computed, which helps to reduce overestimation.

B. Time Uncertainty Transformation

Due to the time transformation that is included in Dromo ODEs, physical time is regarded as a state variable and therefore it is integrated along with the other seven Dromo parameters. From Eqs. (8) and (16) it is clear that the derivative of time with respect to ϕ depends on ζ_{1-3}. Any uncertainty in these variables results into a growing uncertainty in the physical time variable itself. An uncertainty in time is impractical for many applications. A process for obtaining only the position and velocity uncertainty at a specific time t_1 is outlined below.

The uncertainty of the physical time at a given ϕ is represented by the time interval $[\underline{t}, \bar{t}]$. Conversely, a desired time t_1 will be present in a number of solutions for various values ϕ. The first and last of the integrated solutions at ϕ_i $(i = 0, 1, \ldots, N)$ containing t_1 are denoted as:

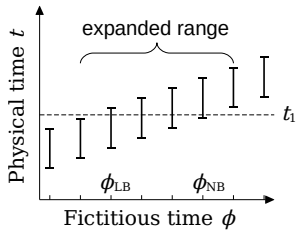

Fig. 2 Proccess for selecting the range of ϕ for removing time uncertainty.

$$\phi_{n_{LB}} = \min_i \phi_i \qquad \phi_{n_{UB}} = \max_i \phi_i \qquad \text{where } t_1 \in [t_i,\, \bar{t}_i] \tag{40}$$

It is important to expand the range outward and include the neighboring solutions of ϕ on the lower and upper bound, such that all solutions between $\phi_{n_{LB}-1}$ and $\phi_{n_{UB}+1}$ are considered. Here $n_X + 1$ and $n_X - 1$ indicate the solutions after and before n_X, respectively. Although intervals t of solutions at $\phi_{n_{LB}-1}$ and $\phi_{n_{UB}+1}$ certainly do not contain t_1, it is not known which solutions in the ranges $[\phi_{n_{LB}-1},\, \phi_{n_{LB}}]$ and $[\phi_{n_{UB}},\, \phi_{n_{UB}+1}]$ might contain t_1. The resulting Cartesian volumes of the integrated solutions between $[\phi_{n_{LB}-1},\, \phi_{n_{UB}+1}]$ need to be joined to get the total verified solution for a given time t_1. The process is illustrated in Fig. 2.

As VSPODE uses a variable step size, subsequent values of ϕ can be far apart. The large spacing results in overestimation in two ways. First, the *a-priori* solution, compared to the tight enclosure, is larger for large step sizes. Only the *a-priori* solution is valid over the ϕ range from one step to the next. Second, all solutions $\phi_{n_{LB}-1}$ until $\phi_{n_{UB}+1}$ have to be considered. At large step sizes, this will likely contain many solutions that do not include t_1. To overcome these issues a refinement is made. The integration is performed again from $\phi_{n_{LB}-1}$ to $\phi_{n_{UB}+1}$ by using a smaller fixed step size. This will produce smaller *a-priori* solutions and discard integration steps that do not contain t_1.

The procedure can even be repeated to further reduce the total volume, albeit at diminishing improvements (reduction of wrapping and narrowing the considered ϕ range) for a given reduction in step size. Each refinement does require additional integration steps and so presents a trade-off between volume and computational effort. On the whole, the number of integration steps required when refining once for a single single time t_1 is likely small, compared to the total number of

integration steps taken from t_0 to t_1. The optimal strategy for refinement will depend on the number of time-certain verified solutions required and depends on the application.

V. Experimental Set-up

The experimental set-up of this study is similar to that of Ref. [6], to be able to compare the Dromo state model directly to the previously obtained results for MEE and USM. Only two uncertainty parameters are included in the study: the atmospheric-density uncertainty factor and the model-error acceleration. The uncertainty parameters and eight uncertainty state variables result in a total of ten uncertainty quantities ($N_u = 10$). These quantities are introduced and discussed in the following sections.

A. Initial State

Two initial uncertainty models are used: the simple and correlated model. In the simple model the initial uncertainty state is modeled as a uniform and uncorrelated six-dimensional distribution in the inertial Cartesian frame. The simple model is included to make the results more comparable to previous studies [6]. Also the initial widths are the same as in Ref. [6]: $10\,\mathrm{m}$ and $0.1\,\mathrm{m\,s^{-1}}$ in the position and velocity components, respectively. The magnitudes are realistic even for very-low orbiting satellites, depending on the measurement type considered [46].

The second correlated initial uncertainty model has two important distinctions: the uncertainties are expressed in the orbital frame and made correlated. The orbital frame is a common reference frame for expressing uncertainty in the state. Specifically, the transverse (or along-track) position uncertainty and radial velocity uncertainty, and radial position uncertainty and transverse velocity uncertainty are inversely correlated [47].

To prevent wrapping the solutions twice, the entire conversion from the uncertainty in the orbital frame to Dromo is executed in one step. This is done by substituting the transformation equations from the orbital frame to the inertial Cartesian frame in the Cartesian to Dromo transformation equations presented in Sec. III.B.3. Moreover, two inversely correlated variables are modeled only by a single initial uncertainty. The two variables are then simply defined as the positive and negative copy of this combined uncertainty variable. This approach reduces the number of uncertain variables

and allows for cancellation.

B. Atmospheric Density

As the research concerns LEO satellites, atmospheric drag needs to be accounted for. A simple tabulated exponential density model, based on U.S. Standard Atmosphere 1976 and CIRA1972 models, is used [48]. A spherical Earth and a co-rotating atmosphere are assumed. The drag acceleration is modeled by:

$$\mathbf{f}_{drag} = -\frac{1}{2}\rho\|\mathbf{v}_{rel}\|\mathbf{v}_{rel}K \tag{41}$$

where the ballistic coefficient is defined as $K = 0.05 \times 10^{-6}\,\mathrm{km}^2\,\mathrm{kg}^{-1}$ [6].

For LEO, atmospheric density is by far one of the most uncertain model parameters. To model this, a random unbiased error of $\pm 20\,\%$ is assumed [6, 49, 50]. The atmospheric drag is modeled as an interval by multiplying the acceleration by an interval factor:

$$\mathbf{F}_{drag} = [0.8,\, 1.2]\mathbf{f}_{drag} \tag{42}$$

C. Gravity Field

Variations in the Earth's gravity field are modeled as a perturbing potential, having contributions to both the perturbing acceleration $\mathbf{f}$ and the potential $\mathcal{U}$. Accounting for oblateness only, the potential and acceleration are given by [45]:

$$\mathcal{U}_{J_2} = \frac{J_2\mu R_E^2}{2r^3}\left(1 - 3\sin^2 i \sin^2(\nu+\omega)\right) \tag{43}$$

$$\mathbf{f}_{J_2} = -\nabla\mathcal{U}_{J_2} \tag{44}$$

where the following constants were assumed [51]: $\mu = 398\,601\,\mathrm{km}^3\,\mathrm{s}^{-2}$, $R_E = 6371.22\,\mathrm{km}$, and $J_2 = 1.082\,65 \times 10^{-3}$. The uncertainty arising from the limited knowledge on the model parameters and limited order and degree of gravity terms are discussed in Sec. V.E.

D. Gravitational Attraction of the Moon

The third-body gravitational attraction by the Moon is modeled. This perturbation is included in most regularized propagation studies [13, 14, 44, 51], but not in the previous study [6]. The third-body perturbation depends explicitly on the physical time, so that the uncertainty related to this variable appears explicitly in the EOMs. This perturbation is implemented in Dromo as derived from a perturbing potential. The perturbing acceleration and the Moon's position in the Earth-centered inertial frame are:

$$\mathbf{f}_M = -\frac{\mu_M}{r_{sM}^2}\mathbf{r}_{sM} \tag{45}$$

$$\mathbf{r}_M = -\frac{1}{2}Q\left[2\sin(\omega t),\, \sqrt{3}\cos(\omega t),\, \cos(\omega t)\right] \tag{46}$$

where $Q = 384\,400\,\mathrm{km}$, $\omega = 2.665\,315\,780\,887 \times 10^{-6}\,\mathrm{rad\,s^{-1}}$, and $\mu_M = 4902.66\,\mathrm{km^3\,s^{-2}}$. The distance vector $\mathbf{r}_{sM} = \mathbf{r}_M - \mathbf{r}_s$ can be obtained from Eqs. (21) and (24). The computation of the potential $\mathcal{U}_M$ and the perturbing accelerations is straightforward. The partial derivative of the potential is:

$$\frac{\partial \mathcal{U}_M}{\partial t} = \frac{1}{2}\mu_M \omega Q \left(\frac{2cR_x + \sqrt{3}R_y + sR_z}{Q^3} - \frac{2ca_X + \sqrt{3}sa_Y + sa_Z}{\left(a_X^2 + a_Y^2 + a_Z^2\right)^{3/2}} \right) \tag{47}$$

where $a_X = R_x - sQ$, $a_Y = R_y + \frac{1}{2}\sqrt{3}cQ$, $a_Z = R_z + \frac{1}{2}cQ$, $s = \sin(\omega t)$, and $c = \cos(\omega t)$.

E. Modeling Errors

The model only includes a limited number of perturbations with a limited fidelity. Moreover, all model parameters (e.g., physical quantities μ and J_2) are only known approximately. To account for both, these contributions are combined into a single additional modeling error acceleration vector, where each component is estimated to be enclosed within $[-10^{-8}, 10^{-8}]\,\mathrm{km\,s^{-2}}$ [6, 52].

It could be beneficial to include unmodeled contributions to the gravity field as an uncertainty interval on top of the J_2 parameter. Dromo treats perturbations arising from a potential separately from other perturbing accelerations. In this way, an uncertainty in a conservative potential will not cause a growth in uncertainty in orbital energy. However, practically this means the introduction

of another uncertainty parameter, which significantly affects the computational efficiency and is therefore not included in this study.

VI. Results

The study investigates TM transformation, a correlated initial interval uncertainty model, and Dromo as a propagation state model. As a result of the chosen state model, a method for removing the time uncertainty by converting it to additional positional and velocity uncertainty is developed. The results of the transformation are separated in the wrapping effect and dependency problem, presented in Secs. VI.A and VI.B. The different initial uncertainty models are compared in Sec. VI.C. In Section VI.D, Dromo is compared against previous state models. The integration of the time uncertainty is detailed in Sec. VI.E. Finally, a sensitivity analysis is presented in Secs.VI.F-VI.H.

A. Transformation Wrapping Effect Overestimation

By using a different state model for the propagation, overestimation is unavoidable and mainly due to two sources: wrapping and dependency. The overestimation due to wrapping represents how much an interval cuboid in one state space remains cuboid in another state space and results from the choice of state models. The overestimation due to dependency measures the complexity of the transformation and also depends on the verified transformation technique.

To better understand the effect of the transformation technique, the wrapping contribution is investigated first. The initial interval state in Cartesian coordinates is transformed to a Dromo initial interval and back. In this process the Cartesian cuboid is wrapped inside a Dromo cuboid, and then wrapped back in a Cartesian cuboid. To negate the dependency problem of the transformation method, the MC method is used for both transformations using 10 000 samples. Figure 3 shows the final interval compared to the original interval. The relative growth with respect to the nominal state (x_0, y_0, z_0) at t_0 is shown.

It can be seen that the initial interval has grown significantly. The final interval has a large spread in the XY- and XZ-plane, but occupies a relatively narrow band in the YZ-plane, causing most of the overestimation due to wrapping of the final Dromo to Cartesian transformation. The shape of the final point cloud appears normally distributed in the three dimensions, while the original

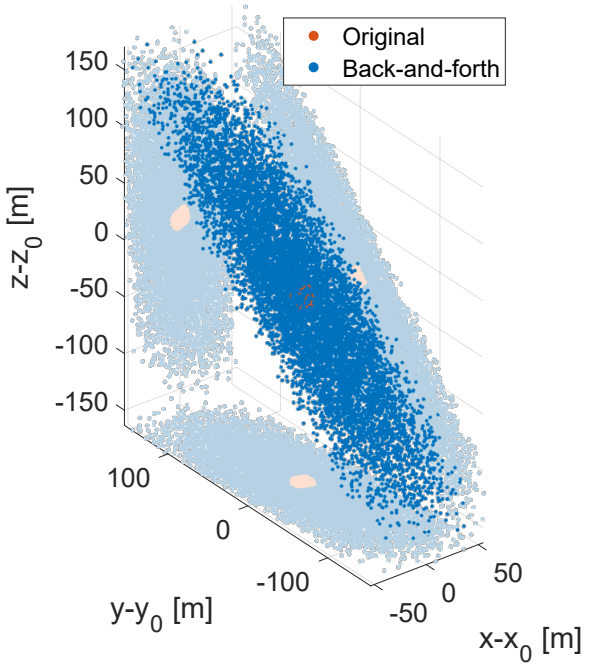

Fig. 3 MC transformation of the initial uncertainty interval from Cartesian to Dromo and back around the initial position at t_0.

point cloud was a cuboid of even density. This change is caused by the transformation equations, in which certain combinations of values are physically not compatible.

The volume of the back-and-forth result is estimated to be $2.48 \times 10^{-3}\,\mathrm{km}^3$ by drawing a convex hull around the samples, while the corresponding cuboid measures $11.12 \times 10^{-3}\,\mathrm{km}^3$. The overestimation due to wrapping is thus a factor 4.48. In a similar fashion, the overestimation of the velocity volume is by a factor 3.36. These factors are small compared to the overestimation due to dependency and thus the total overestimation. Nonetheless, wrapping occurs at every integration step. This illustrates the downside of verified propagation in Cartesian space. The ellipsoid rotates 360 deg every orbit and is wrapped by a Cartesian cuboid at each step.

To investigate the wrapping in the Dromo space the volume of the samples is estimated by fitting a three-dimensional and four-dimensional convex hull around ζ_{1-3} and ζ_{4-7}, respectively. The volume of the convex hull is compared to the volume of the cuboid interval to obtain an overestimation factor. The obtained (hyper)ellipsoid volumes are extremely small compared to the cuboid volumes and nearly zero. Due to limited machine precision, computing an exact overestimation factor is nonsensical, so it can only be noted that the overestimation due to wrapping is very significant.

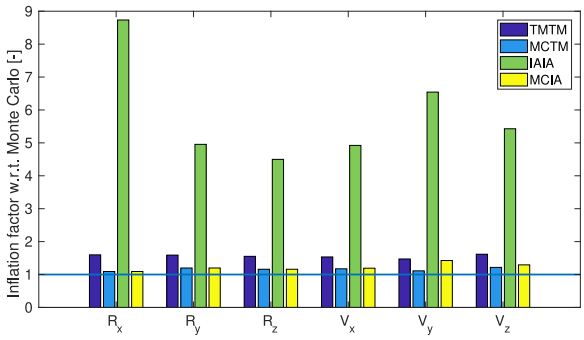

Fig. 4 Inflation factor of the initial uncertainty interval with respect to MC for both directions, using TM for both directions (TMTM), TM only for Dromo back to Cartesian (MCTM), IA for both directions (IAIA), and lastly IA only for the transformation back to Cartesian (MCIA).

Comparing the wrapping effect of the transformation from Cartesian to Dromo, and also Dromo back to Cartesian, the major part of the wrapping effect is caused in the initial transformation. Nevertheless, the overestimation due to wrapping is still 300 times smaller compared to the same transformation for USM and MEE [6].

B. Transformation Dependency Problem Overestimation

The second source of overestimation due to transformation is the dependency problem, which depends on the interval technique used. In Ref. [6], standard IA is used for both directions of the transformation between Cartesian and Dromo variables. For this study TM transformations are implemented and compared against IA. To differentiate between both directions of transformation, the verified methods are used for the entire forth-and-back transformation and also starting from the previous MC interval solution in Dromo state space. The MC solution, which already accounts for the wrapping effect, is used as a baseline for the transformation. For the TM transformations, a TM order of $q = 4$ and tolerance of $\epsilon = 10^{-16}$ are used. The result of the comparison is shown in Fig. 4.

The figure shows the interval inflation factor as the transformed Cartesian interval width divided by the MC interval width obtained earlier. The inflation factor of the Cartesian coordinates is between five and nine when IA is used for both transformations. The inflation in x-direction is largest, which is approximately in the cross-track direction in this particular example. Overall,

the inflation is roughly similar for each of the Cartesian components. Comparing the different techniques, TM transformation provides significantly better results than IA and is close to the MC transformation. The final position volume of the TM solution is four times the MC volume, compared to an increase of a factor 195 for IA.

Both techniques perform significantly better on the Dromo-to-Cartesian transformation than vice-versa, as illustrated by the MCTM and MCIA results. This further indicates that the initial transformation introduces the most overestimation. The final Cartesian position volumes of MCTM and MCIA are both 152% larger than MCMC. The velocity volumes are larger than the position volumes for both techniques, with also a larger difference between the two: 220 % for MCTM and 435 % for MCIA compared to MCMC.

The significantly smaller volumes for MC suggest that applications where the initial conditions are obtained from empirical data would benefit from transforming the data to the propagation state model directly, before computing the initial intervals. In conclusion, the final volume of the TM transformation, back to Cartesian space, is $0.044\,\mathrm{km}^3$, which is roughly four orders of magnitude larger than the initial volume of $1 \times 10^{-6}\,\mathrm{km}^3$. Much of the overestimation is due to the inherent wrapping effect of the chosen Dromo state model. This is unavoidable, when the model is used for propagation. Nonetheless, this is four orders of magnitude smaller than the starting volumes of the MEE and USM state models used in Ref. [6], as shown in Sec. IV.A.

C. Initial Interval Models

The correlated initial uncertainty model assumes a dependency between uncertainty in the state variables. The marginal distributions and thus intervals remain exactly the same as the simple (uncorrelated) model. The usage of fully correlated variables reduces the number of uncertain variables, simplifying the transformation problem and allowing for additional cancellation and removal of dependency when the tighter enclosure is computed. To compare the effect of correlated uncertainty among variables, the uncertainties in the transverse position and radial velocity, and radial position and transverse velocity are assumed to be correlated with a correlation coefficient $\rho = -1$ [47]. This reduces the number of uncertain parameters from six to four.

To benefit from this reduction, the entire initial uncertainty transformation from the orbital

frame to inertial Cartesian coordinates and Cartesian coordinates to Dromo elements is combined into a single transformation. The correlation is not carried on through the propagation and only affects the first transformation, which was previously shown to cause the largest overestimation. A reduction in width of all Dromo elements, compared to the uncorrelated situation, is observed. The interval width of the elements is reduced by a factor between 1.3 and 4.4. This reduction is quite significant, considering that the marginal distributions are identical. The correlated samples have roughly similar orbital energy and thus produce smaller initial Dromo intervals. Transformed back to Cartesian coordinates, the resulting position and velocity volumes are a factor 1.7 and 1.9 smaller, when correlations are introduced.

D. Comparison with Other State Models

Two initial uncertainty models are used for the comparison. The first is the simple initial uncertainty model, which is also used for MEE and USM in Ref. [6]. However, this model gives much smaller starting intervals when using TM transformations with Dromo compared to Ref. [6], in which IA transformations were used for both state models. To account for this, a second model is introduced that inflates the initial Cartesian uncertainty by a factor 25, such that the forth-and-back Cartesian position volume is $688\,\mathrm{km}^3$ and roughly equal to that obtained with MEE and USM. In this way differences between Dromo x25, MEE, and USM are due to the propagation stability only.

The verified orbit is propagated until solution explosion, for both initial uncertainty models and compared to the previous values shown in Fig. 1. The settings for VSPODE are as follows: $q = 3$, $k = 16$, and $\epsilon = 10^{-14}$. These settings (or tuning parameters) are introduced in Sec. II.C. The comparison with Cartesian, MEE and USM state models is shown in Fig. 5.

Dromo with the uncorrelated TM initial volume is able to propagate for almost 300 hours until interval explosion, whereas the Dromo x25 model is able to propagate for almost 200 hours. This is much longer that the previously obtained durations of 5, 30, and 35 hours for Cartesian, MEE, and USM, respectively. Dromo is able to provide a stable verified propagation, which is at least five times longer with respect to that obtained with the other state models. For applications, such as conjunction analysis, this allows a significantly longer forecasting period.

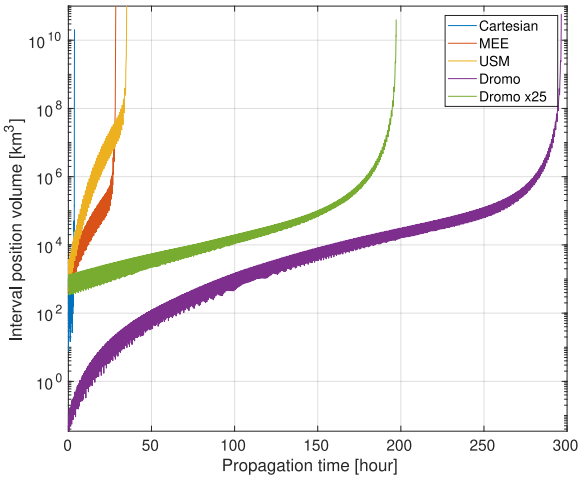

Fig. 5 Position interval volume growth with propagation time for the Cartesian, MEE, USM, and Dromo state models.

E. Time Transformation

A Dromo interval solution at a given ϕ has an uncertainty in both Cartesian coordinates and time. For most analyses, this time uncertainty is often undesirable. To construct an interval of position and velocity only for a given epoch, a range of integrated solutions needs to be considered. The developed process is discussed in Sec. IV.B. A target epoch of $t_1 = 10\,\text{h}$ is chosen for the x25 Dromo propagation. The first integrated solution containing t_1 has a time interval width of $w(t) = 62.4\,\text{s}$ and is shown in Fig. 6. The interval solutions are shown as the result of three levels of refinement. The third refined level with step size $h_\phi = 0.001$ is considered the final and desired Cartesian interval.

In the first unrefined level, the total Cartesian interval is obtained by finding all integrated solutions that contain t_1 and expanding the range of solution outward. Although the two outer integrated solutions do not contain t_1, they are included, as it cannot be known which solutions in-between do contain the target time. The downside of the result from the first unrefined level is that it produces large overestimation when joined. As the step size is large, the range in ϕ is also large. A better result is obtained when the step size is refined.

For the second level (now including refinement), the integration is restarted at each of the previous integrated solutions and propagated to the next with a fixed step-size of $h_\phi = 0.01$. The process of selecting only the integrated solutions that contain the target time and the expansion of

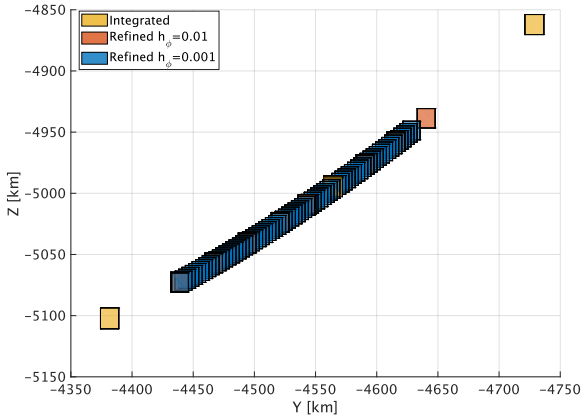

Fig. 6 Interval solutions of the variable step-size integration and two refinements around the target time t_1 of 10 hours.

the range is repeated. As a result of the finer spacing, 6 out of the 15 new solutions are discarded, giving a narrower range in ϕ.

For the third level, the same process of refinement is repeated, but with an even finer step size of $h_\phi = 0.001$. Out of the 78 solutions, 73 contain t_1 or are at the boundaries. A further refinement can be made, if required. To obtain the final verified Cartesian interval at the specified time t_1, the *a-priori* solutions of each of the 73 solutions are joined.

A major advantage of this method is that the final verified Cartesian interval consists of a large number of individual solutions, allowing for more complex shapes than a single six-dimensional interval cuboid. In many cases, such as in this example, a single cuboid would have a large overestimation due to wrapping: a single cuboid wrapping all 73 sub-intervals is $3.5 \times 10^7\,\mathrm{km}^3$, compared to $1.4 \times 10^5\,\mathrm{km}^3$ for a union of the sub-intervals, as estimated by fitting a convex hull around all the corner coordinates. The overestimation due to wrapping is almost a factor 250.

The large cuboid and the set of smaller ones can be used for further analysis, including conjunction analysis. For instance, if an intersection between the large cuboid of two objects is detected, a more refined comparison between the respective smaller cuboids can be made. The process of computing interval intersections and collision predictions is treated in Ref. [6].

The shown intervals are nearly square in the $yz-$plane and very small in the along-track direction, even if this direction contains most of the uncertainty. By studying the contribution of Dromo

elements on the positional uncertainty, it is found that the along-track uncertainty is almost entirely absorbed by the time uncertainty. So while the ODE of this element is directly dependent on other elements, it has only a marginal effect on the overall system through the third-body perturbation of the Moon. This allows the regularized formulation to remain stable for so long.

F. Sensitivity of the Propagation Time to Tuning Parameters

This section describes the different tuning parameters and how they affect the propagation using Dromo and is followed by a sensitivity study. For certain combinations of the tuning parameters, VRIOP sometimes produces significantly worse results, despite only small changes to the parameters, creating plateaus of *successful* combinations in the tuning-parameter space. This instability has been noted in Ref. [6] and will be demonstrated and discussed further.

The ITS order k presents a trade-off between computational efficiency and numerical sensitivity. A high value of k tends to be much more computationally efficient. At higher orders the step-size can often be made very large, at the cost of introducing numerical sensitivity in the higher-order terms. The coefficients of the higher-order terms become very small, while the independent variable is raised to a high exponent. Also, in practice, a satellite orbit model is only continuously differentiable by approximation. For instance, the atmospheric density results from a tabulated model. This trade-off holds true for Taylor-series integration of satellite trajectories in general [53]. Ref. [23] also notes a worsening in breakdown time on the Lotka-Volterra problem for increasing order k. The larger steps result in a slight increase in overestimation in the tightened solutions and thus shorter propagation time until explosion.

A higher TM order q generally results in a higher accuracy and longer propagation time until explosion, at the cost of numerical efficiency and sensitivity. The computational cost is roughly raised to the power of $N_u q$, where N_u is the number of uncertain quantities (state variables and model parameters). As q increases, the success of a run becomes very sensitive to the other parameters and initial conditions.

Finally, the numerical tolerance ϵ directly drives the step-size control. Due to the large model uncertainty and overestimation, the numerical accuracy has only a small effect on the solution and thus time until interval explosion. However, it still significantly impacts the computational efficiency.

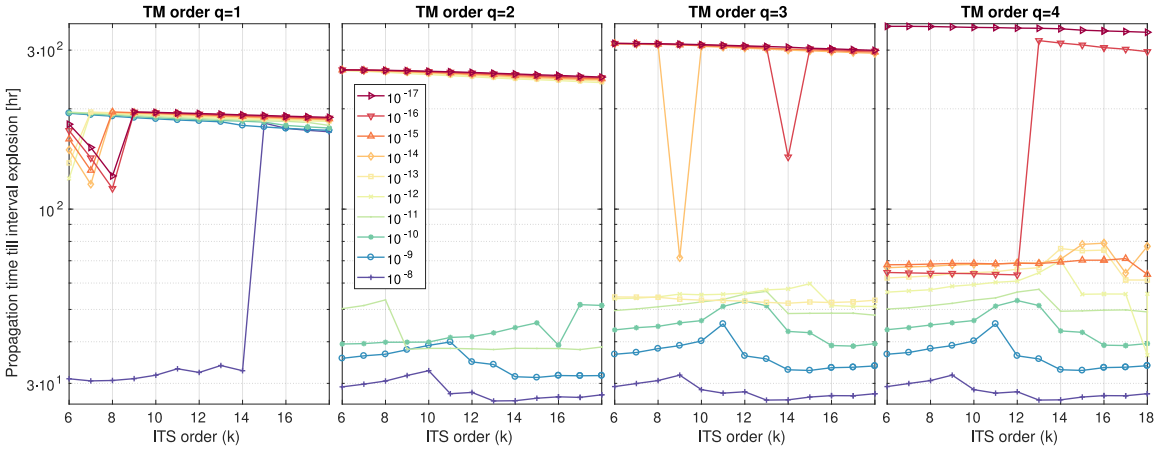

Fig. 7 Sensitivity of propagation time to various combinations of the tuning parameters: TM order q, ITS order k, and tolerance ϵ.

Also, the numerical tolerance generally needs to be large for high values of q, to produce successful runs.

The following ranges of parameters are investigated: $k \in [6,\ 18]$, $q \in [1,\ 4]$, and $\epsilon \in [10^{-8},\ 10^{-17}]$. Also $q = 5$ and 6 were considered, but no successful results could be obtained even with very tight tolerances. Moreover, tighter tolerances such as $\epsilon = 10^{-18}$ and 10^{-19} produced results similar to 10^{-17}, at higher computational cost. Tolerances beyond 10^{-16} are below double precision, however the VSPODE solver produces different solutions for all mentioned tolerances, suggesting different behavior of the step-size control algorithm. This is especially clear for order $q = 4$, as will be demonstrated.

Figure 7 shows the result of the propagation time in hours until interval explosion for a range of tuning parameters. The best propagation results are obtained for the TM order $q = 4$, with the ITS order $k = 8$ and tolerance $\epsilon = 10^{-17}$. The resulting propagation time until interval explosion is 354 h.

From the graphs it can be seen that an increase in the TM order results in a longer propagation time. The relative increase in additional propagation time with increasing order q is 24% ($q = 2$ to 3), 20% ($q = 3$ to 4) and 12% ($q = 3$ to 4). The gain in additional propagation time thus seems to converge. There exists a clear separation in propagation time between successful and unsuccessful combinations of the tuning parameters, which is roughly a factor 5. The number of successful

solutions decreases with the TM order q. Moreover, no successful runs for orders 5 and 6 were obtained within the given parameter space.

It can further be seen that the propagation time decreases slightly with increasing integration order. This is due to overestimation remaining after computing the tighter enclosure, also noted in Ref. [23]. The decrease from order $k = 6$ to 18 is less than 5 %. For certain choices of the tuning parameters, k is important in achieving successful runs. Some drops in lines of solutions with varying k can also be observed for $q = 1$ and 3. For the former there is a clear pattern. This phenomenon is also observed by Ref. [6]. These solutions are only slightly unstable, within a stable region of the tuning-parameter space.

The numerical tolerance has little effect on the actual propagation time amongst successful runs, especially below the value of $\epsilon = 10^{-12}$. More stringent tolerance settings are required to produce successful runs of higher orders of q.

Without performing a computationally costly survey of the tuning parameter space, it is advised to start with a low TM order, combined with high ITS order and medium tolerance, for example, $k = 16$ and $\epsilon = 10^{-14}$. Such a combination tends to produce the most robust results and is also computationally favourable (as will be discussed next).

G. Sensitivity of CPU Time to Tuning Parameters

The corresponding CPU simulation time to obtain the results of Fig. 7 are shown in Fig. 8. The sensitivity study is entirely performed on an Intel i7-4712HQ CPU at 2.30 GHz with a maximum Turbo frequency of 3.30 GHz.

There is a wide spread of CPU simulation time and there is still a clear separation between successful and unsuccessful runs, although the distinction is less pronounced. The relationship between propagation time until explosion and CPU simulation time is strongly non-linear. For instance, the solution with the best result (longest propagation time) took 185 092 s (or 51.4 h), while the successful solution that required the shortest computation time was obtained with $q = 1$, $k = 16$ and $\epsilon = 10^{-8}$ and took a total of 225 s to complete for a propagation time of 172 h. Therefore, increasing the propagation time by a factor two comes at the expense of increasing the computational cost by a factor 323.

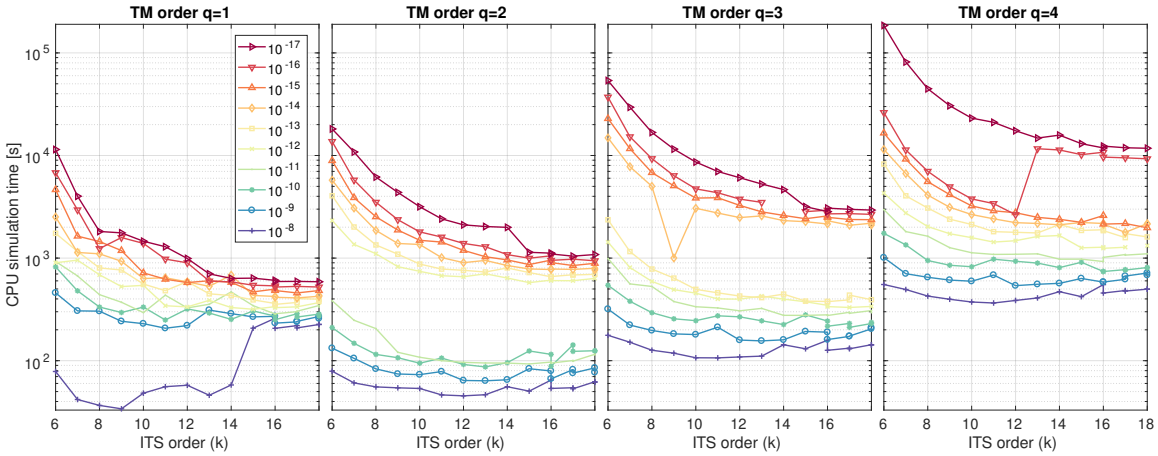

Fig. 8 Sensitivity of CPU simulation time to various combinations of the tuning parameters: TM order q, ITS order k, and tolerance ϵ.

The ITS order k also has a strong effect on the computational cost, which is inversely related to the order. Comparing the solutions obtained with order $k = 6$ and 18, the decrease in computational cost is roughly a factor 18 for all TM orders, considering only the successful runs. The propagation time until explosion only marginally decreases, while providing more successful solutions. So, higher orders of k are recommended. Small values of k should be considered when a dense history of solutions is desirable.

Finally, a good trade-off for the numerical tolerance is more difficult to obtain. In contrast to the propagation time, there is quite a significant spread among the different tolerance settings for a given value of q. More stringent tolerances significantly increase the computational load at almost no improvement in propagation time. The least stringent tolerance for a given combination of k and q, while producing successful results, is thus most favorable. The CPU simulation time decreases with increasing ITS order k. Also, high values of TM order q require more stringent tolerances.

H. CPU Time versus Propagation Time

To better understand the trade-off between solution stability and computational effeciency, the same results as shown in Figs. 7 and 8 are combined to construct a Pareto front shown in Fig. 9.

A line is fitted to approximate the Pareto frontier, solutions to the bottom and/or right of this line are likely to be infeasible. The groups of successful solutions belonging to each of the TM

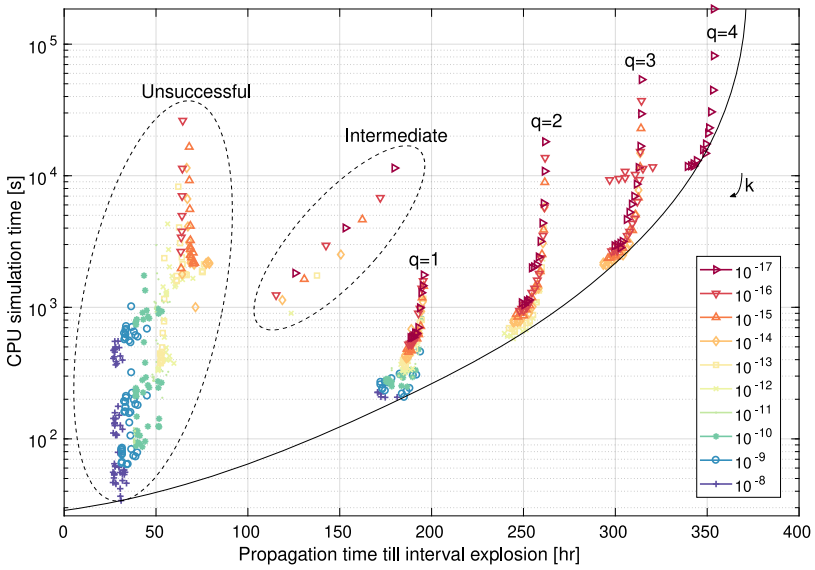

Fig. 9 CPU simulation time compared to propagation time for various combinations of the tuning parameters: TM order q, ITS order k, and tolerance ϵ.

order q are clearly identifiable and separated. Varying order k creates hockey-stick patterns, with increasing order towards the bottom. The only exceptions are some solutions with $q = 4$, $\epsilon = 10^{-16}$, which are intersecting the group of solutions obtained with $q = 3$.

The unsuccessful solutions are also clearly separate from successful solutions. Groups of constant order q of unsuccessful solutions are less distinct, due to the invariance of propagation time with q for this group. So, if the propagation time until solution explosion does not improve with increasing order q, it can be that only unsuccessful solutions are generated.

The intermediate solutions are also a distinctly separate group. These present solutions that are generally within a successful region of the tuning-parameter space, but perform worse than neighboring solutions. These are also visible in Fig. 7 and previously discussed. The figure further confirms that even higher orders of q will likely only produce unsuccessful runs or only a small improvement in propagation time at a large computational cost.

I. Orbital Sensitivity

To further investigate the sensitivity of the propagation time, a study across various orbits is conducted. The perigee altitude h_p, eccentricity e, and inclination i are varied. The initial uncertainty remains the same in each case. The various choices for the orbital parameters are:

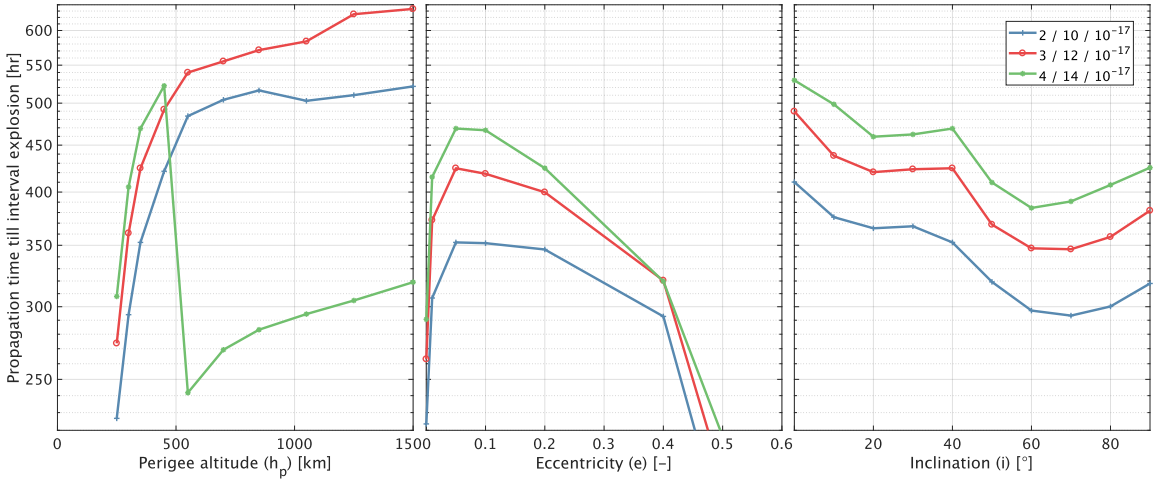

Fig. 10 Sensitivity of propagation time to orbital parameters.

$$h_p \in \{250,\ 300,\ 350,\ 450,\ 550,\ 700,\ 850,\ 1050,\ 1250,\ 1500\}$$

$$e \in \{0.0001,\ 0.01,\ 0.05,\ 0.1,\ 0.2,\ 0.4,\ 0.7,\ 0.9,\ 0.95,\ 0.99\}$$

$$i \in \{0,\ 10,\ 20,\ 30,\ 40,\ 50,\ 60,\ 70,\ 80,\ 90\}$$

To limit the number of runs, the orbital parameters are varied only one parameter at a time with respect to a nominal orbit: $h_p = 350\,\text{km}$, $e = 0.05$, and $i = 40°$. So 28 simulations are performed for three sets of tuning parameters. Following the results of Secs. VI.F and VI.G, the following combinations of $q/k/\epsilon$ are investigated: $2/10/10^{-17}$, $3/12/10^{-17}$, and $4/14/10^{-17}$. The results of this study are shown in Fig. 10.

Looking at the perigee altitude, the propagation time until solution explosion initially strongly grows with increasing altitude, which is explained by the reduction in atmospheric density and the diminishing effects of the oblate gravity model. Above 550 km the rate of increase is milder. For the setting $4\,/\,14\,/\,10^{-17}$, no successful solutions were obtained beyond 450 km. Several values of k and ϵ were seen to not avail. It is clear that a complex TM with a high order increases the propagation time until explosion, but also results in a more sensitive solution. For higher orbits, it is advisable to not model the atmospheric density separately, but to include it in the combined uncertainty acceleration, as discussed in Sec. V.E. For the other two settings, the propagation continues to increase with h_p; the maximum propagation time achieved is 633 h.

Considering the orbital eccentricity, the propagation time is improved with increasing order, which is to expected. At the altitude of the nominal orbit all three settings are equally stable. Slightly eccentric orbits ($e = 0.05$) produce more stable solutions than nearly circular orbits ($e = 0.0001$). Results are obtained to about an eccentricity of 0.4, where the propagation time is 25 % less than at $e = 0.05$. Instead of the tabulated atmosphere model, a continuously differentiable model could be used when the orbit is very eccentric [53].

Finally, looking at the inclination, there is a clear and similar trend for each of the three settings. Compared to the maximum propagation time at 0° inclination, the minimum is about 28 % lower and occurs between $i = 60°$ and 70°. The propagation time increases again towards $i = 90°$. This dependency is caused by the oblate gravity field. Perturbations to the orbital plane due to the J_2-term are known to have the largest magnitude between $i = 45°$ and 90°. For the values of eccentricity and perigee altitude of the nominal orbit, the variation in inclination has no effect on the solution stability.

The different settings presented here and many more attempted in trial and error, further illustrate the sensitivity of VRIOP to its tuning parameters, especially for higher values of the TM order q. To achieve a robust set of tuning parameters across a different range of orbital parameters, a trade-off between propagation time, computational cost, and sensitivity needs to be made. From the wide range of values studied, the following settings are recommended: $q = 3$, $k = 12$, and $\epsilon = 10^{-17}$.

VII. Conclusions

The proposed Dromo state model and Taylor Model (TM) transformation method for the verified interval orbital propagation (VIOP) result in a much more stable state model, compared to previously investigated models. For comparison, a satellite in a circular low-Earth orbit (LEO) at 400 km is propagated, including perturbations caused by the atmosphere and the oblate gravity field. Dromo is able to propagate for almost 300 h until solution explosion, compared to 5, 30, and 35 h for Cartesian, MEE, and USM, respectively. This results is due to a smaller initial uncertainty volume and better propagation stability. Starting from a comparable initial uncertainty volume the resulting propagation time is nearly 200 h.

Wrapping of the Cartesian intervals in the Dromo space is found to be the primary source of overestimation in the transformation. Wrapping of Dromo intervals back in Cartesian space inflates the position and velocity volumes by a factor 4.5 and 3.4, respectively. TM transformation produces significantly less overestimation than interval analysis (IA) transformation. The total initial positional uncertainty overestimation is reduced by a factor 1600 compared to previous studies. Compared to Monte Carlo (MC) (i.e., overestimation due to dependency only), the position volumes of a back-and-forth transformation using TM and IA are 4 and 195 times larger, respectively. When both TM and IA are used to only transform the intermediate MC result back to the Cartesian space, the resulting inflation is only 1.5 for both. This shows that the Cartesian-to-Dromo transformation introduces most of the overestimation.

The uncertainty in the time state variable is initially zero, but is shown to quickly grow in interval width and to acquire much of the uncertainty present in the along-track direction. This allows for a very good representation and absorption of the orbital uncertainty. Moreover, it improves the stability of the integration, as the physical time has only marginal influence on the other elements.

To remove time uncertainty from the verified solutions a process for transforming it into additional position and velocity uncertainty has been proposed and demonstrated. To remain verified, the solution needs to consider a wide range of ϕ, which introduces additional overestimation. This overestimation can be reduced by re-integrating sections of the trajectory with a finer and fixed step-size $\Delta\phi$.

A study has been conducted to analyze the sensitivity of verified regularized interval orbit propagation (VRIOP) to tuning parameters: the Taylor-expansion order of integration k, the TM order q, and the numerical tolerance ϵ. The propagation time until solution explosion is found to vary between 172 h and 354 h for a LEO satellite. Generally, the propagation time increases with a higher TM order q, but at a diminishing rate, increasing 24, 20 and 12% changing q from 1 to 4. The propagation time is slightly negatively correlated with the expansion order k of the integration: less than 5 % from $k = 6$ to 18. The propagation is hardly affected by the numerical tolerance ϵ, especially below 10^{-14}.

Certain regions of the tuning space are shown to produce many unsuccessful solutions, which

generally abort integration at 15 % of the propagation time, compared to neighboring successful solutions. Higher TM orders q are more sensitive and require more stringent tolerance settings and higher values of ITS order k. No successful solutions are obtained for order $q = 5$ and higher. For unsuccessful runs the propagation time does not vary with q and can serve as indication of an unsuccessful region of the tuning-parameter space.

The CPU time is found to have a large spread for all tuning parameters, varying from minutes to days in length. The CPU time increases to a power of q, is inversely proportional to the numerical tolerance, and exponentially decays with k. Considering the small impact of k and ϵ on the propagation time and the diminishing return with increasing values of q, the following settings are recommended: $q = 3$, $k = 12$, and $\epsilon = 10^{-17}$.

Finally, the sensitivity to the perigee altitude, eccentricity and inclination are investigated. For nearly circular orbits, a higher altitude results in increased propagation time up to 633 h at $h_p = 1500$ km. The TM order $q = 4$ is not able to provide successful solutions beyond $h_p = 450$ km. This is likely due to overmodeling of the increasingly unperturbed motion. The removal of the atmospheric density as an uncertain parameter is then recommended. Eccentricities beyond $e = 0.4$ did not produce any satisfactory results, which is likely due to solution steps far transcending the altitude brackets of the tabulated atmosphere model. For the inclination, there is a variation of 28 % in propagation time with respect to the maximum at $i = 0°$, but viable solutions are obtained over the entire range.

The propagation time of VRIOP is almost 10 times longer than previously obtained in literature. The maximum forecasting window of verified solutions ranges from several days to nearly a month, depending on the integrator settings, orbital regime, and initial uncertainty. Thus Dromo greatly increases the applicability of VRIOP to conjunction analyses and other SSA activities, especially where verified solutions are required or can provide additional advantages.

Acknowledgements

This work is supported by the U.S. Air Force European Office for Aerospace Research and Development (EOARD), grant FA9550-14-1-0344.

References

[1] Klinkrad, H., "The Current Space Debris Environment and its Sources," *Space Debris - Models and Risk Analysis*, edited by H. Klinkrad, chap. 2, Springer Verlag, Berlin, 2006, pp. 5–58.

[2] Patera, R. P., "General method for calculating satellite collision probability," *Journal of Guidance, Control, and Dynamics*, Vol. 24, No. 4, 2001, pp. 716–722, doi: 10.2514/2.4771.

[3] Klinkrad, H., Alacrón, J., and Sánchez, N., "Collision Avoidance for Operational ESA Satellites," *European Conference on Space Debris*, 2005, pp. 509–515.

[4] Klinkrad, H., Alarcón, J., and Sánchez, N., "Operational Collision Avoidance with Regard to Catalog Objects," *Space Debris - Models and Risk Analysis*, edited by H. Klinkrad, chap. 8, Springer Verlag, Berlin, 2006, pp. 215–240.

[5] Mason, J., Stupl, J., Marshall, W., and Levit, C., "Orbital debris–debris collision avoidance," *Advances in Space Research*, Vol. 48, No. 10, 2011, pp. 1643–1655, doi: 10.1016/j.asr.2011.08.005.

[6] Römgens, B., Mooij, E., and Naeije, M., "Satellite collision avoidance prediction using verified interval orbit propagation," *Journal of Guidance, Control, and Dynamics*, Vol. 36, No. 3, 2013, pp. 821–832, doi: 10.2514/1.57888.

[7] Celletti, A. and Chierchia, L., "On the stability of realistic three-body problems," *Communications in Mathematical Physics*, Vol. 186, No. 2, 1997, pp. 413–449, doi: 10.1007/s002200050115.

[8] Hoefkens, J., Berz, M., and Makino, K., "Controlling the wrapping effect in the solution of ODEs for asteroids," *Reliable Computing*, Vol. 9, No. 1, 2003, pp. 21–41, doi: 10.1023/A:1023009910949.

[9] Alessi, E. M., Farres, A., Jorba, À., Simo, C., Vieiro, A., and Summerer, L., "Efficient usage of self validated integrators for space applications," *ESA and Universitat de Barcelona TR-07/5202, Barcelona, Spain*, 2007.

[10] Armellin, R., Morselli, A., Di Lizia, P., and Lavagna, M., "Rigorous computation of orbital conjunctions," *Advances in Space Research*, Vol. 50, No. 5, 2012, pp. 527–538, doi: 10.1016/j.asr.2012.05.011.

[11] Urrutxua, H., Souied, Y., and Peláz, J., "Sensitivity Analysis of Regularized Orbit Formulations with Interval Arithmetic," *Advances in the Astronautical Sciences*, Vol. 168, 2019, pp. 1157–1172.

[12] Valli, M., Armellin, R., Di Lizia, P., and Lavagna, M. R., "Nonlinear Mapping of Uncertainties in Celestial Mechanics," *Journal of Guidance, Control, and Dynamics*, Vol. 36, No. 1, 2013, pp. 48–63, doi: 10.2514/1.58068.

[13] Geul, J., Mooij, E., and Noomen, R., "Regularised methods for high-efficiency propagation," *Proceedings of the 2015 AAS/AIAA Specialist Conference, Vail, CO, USA*, 2015, pp. 4105–4124.

[14] Baù, G., Bombardelli, C., and Peláez, J., "A New Set of Integrals of Motion to Propagate the Perturbed Two-body Problem," *Celestial Mechanics and Dynamical Astronomy*, Vol. 116, No. 1, 2013, pp. 53–78, doi: 10.1007/s10569-013-9475-x.

[15] Hoefkens, J., *Rigorous numerical analysis with high-order Taylor models*, PhD thesis report, Michigan State University. Department of Mathematics, 2001.

[16] Moore, R. E., *Interval analysis*, Vol. 4, Prentice-Hall Englewood Cliffs, NJ, 1966.

[17] Moore, R. E., "Interval arithmetic," *Interval analysis*, Vol. 4, chap. 1, Prentice-Hall Englewood Cliffs, NJ, 1966, pp. 8–14.

[18] Makino, K., *Rigorous analysis of nonlinear motion in particle accelerators*, PhD thesis report, Michigan State University. Dept. of Physics and Astronomy, 1998.

[19] Berz, M. and Makino, K., "New methods for high-dimensional verified quadrature," *Reliable Computing*, Vol. 5, No. 1, 1999, pp. 13–22, doi: 10.1023/A:1026437523641.

[20] Neumaier, A., "Taylor forms - use and limits," *Reliable computing*, Vol. 9, No. 1, 2003, pp. 43–79, doi: 10.1023/A:1023061927787.

[21] Makino, K. and Berz, M., "Taylor model range bounding schemes," *Third International Workshop on Taylor Methods, Miami Beach, FL*, 2004, pp. 1–70.

[22] Nedialkov, N. S., "Interval Tools for ODEs and DAEs," *Scientific Computing, Computer Arithmetic and Validated Numerics*, 2006, pp. 35–46, doi: 10.1109/SCAN.2006.28.

[23] Lin, Y. and Stadtherr, M. A., "Validated Solutions of Initial Value Problems for Parametric ODEs," *Applied Numerical Mathematics*, Vol. 57, No. 10, 2006, pp. 1145–1162, doi: 10.1016/j.apnum.2006.10.006.

[24] Nedialkov, N. S., Jackson, K. R., and Corliss, G. F., "Validated solutions of initial value problems for ordinary differential equations," *Applied Mathematics and Computation*, Vol. 105, 1999, pp. 21–68, doi: 10.1016/S0096-3003(98)10083-8.

[25] Eble, I., *Über Taylor-Modelle*, PhD thesis report, Universität Karlsruhe, 2007.

[26] Auer, E. and Rauh, A., "VERICOMP: a system to compare and assess verified IVP solvers," *Computing*, Vol. 94, No. 2-4, 2012, pp. 163–172, doi: 10.1007/s00607-011-0178-4.

[27] Wakker, K. F., "Regularization," *Fundamentals of Astrodynamics*, chap. 10, Institutional Repository Delft University of Technology, 2015, pp. 219–242.

[28] Kustaanheimo, P. and Stiefel, E., "Perturbation Theory of Kepler Motion based on Spinor Regularization," *Journal für die Reine und Angewandte Mathematik*, Vol. 1965, No. 218, 1965, pp. 204–219, doi: 10.1515/crll.1965.218.204.

[29] Burdet, C. A., "Regularization of the Two Body Problem," *Zeitschrift für Angewandte Mathematik und Physik*, Vol. 18, No. 3, 1967, pp. 434–438, doi: 10.1007/BF01601283.

[30] Waldvogel, J., "Quaternions and the perturbed Kepler problem," *Celestial Mechanics and Dynamical Astronomy*, Vol. 95, No. 1-4, Aug 2006, pp. 201–212, doi: 10.1007/s10569-005-5663-7.

[31] Fukushima, T., "New Two-body Regularization," *The Astronomical Journal*, Vol. 133, No. 1, 2007, pp. 1–10, doi: 10.1086/509606.

[32] Fukushima, T., "Numerical Comparison of Two-body Regularizations," *The Astronomical Journal*, Vol. 133, No. 6, 2007, pp. 2815–2824, doi: 10.1086/518165.

[33] Waldvogel, J., "Fundamentals of Regularization in Celestial Mechanics and Linear Perturbation Theories," *Fundamentals of Regularization in Celestial Mechanics and Linear Perturbation Theories*, 2007, pp. 168–184, doi: 10.1201/b10365-14.

[34] Peláez, J., Hedo, J. M., and Rodríguez de Andrés, P., "A Special Perturbation Method in Orbital Dynamics," *Celestial Mechanics and Dynamical Astronomy*, Vol. 97, No. 2, 2007, pp. 131–150, doi: 10.1007/s10569-006-9056-3.

[35] Waldvogel, J., "Quaternions for Regularizing Celestial Mechanics - the Right Way," *Celestial Mechanics and Dynamical Astronomy*, Vol. 102, 2008, pp. 149–162, doi: 10.1007/s10569-008-9124-y.

[36] Baù, G. and Bombardelli, C., "Time Elements for Enhanced Performance of the Dromo Orbit Propagator," *The Astronomical Journal*, Vol. 148, No. 3, 2014, pp. 43–58, doi: 10.1088/0004-6256/148/3/43.

[37] Ferràndiz, J., "A General Canonical Transformaiton Increasing the Number of Variables with Application to the Two-body Problem," *Celestial Mechanics*, Vol. 41, No. 1968, 1988, pp. 343–357, doi: 10.1007/BF01238770.

[38] Amato, D., *Advanced orbit propagation methods applied to asteroids and space debris*, PhD thesis report, Universidad Politécnica de Madrid, Departamento de Física Aplicada a las Ingenierías Aeronáutica y Naval, 2017.

[39] Hernando-Ayuso, J., Bombardelli, C., and Baù, G., "Uncertainty propagation in the N-body problem using Dromo elements," *Acta Astronautica*, Vol. 156, 2019, pp. 252–261, doi: 10.1016/j.actaastro.2017.12.030.

[40] Jezewski, D. J., "A Comparative Study of Newtonian, Kustaanheimo/Stiefel, and Sperling/Burdet Optimal Trajectories," *Celestial Mechanics*, Vol. 12, No. 3, 1975, pp. 297–315, doi: 10.1007/BF01228565.

[41] Stiefel, E. and Scheifele, G., "Typical perturbations," *Linear and Regular Celestial Mechanics*, chap. 5, Springer-Verlag, 1971, pp. 73–125.

[42] Vittaldev, V., Mooij, E., and Naeije, M. C., "Unified State Model theory and application in Astrodynamics," *Celestial Mechanics and Dynamical Astronomy*, Vol. 112, No. 3, 2012, pp. 253–282, doi: 10.1007/s10569-011-9396-5.

[43] Bond, V. R. and Allman, M. C., "Special perturbation methods," *Modern Astrodynamics*, chap. 9, Princeton University Press, 1996, pp. 147–183.

[44] Bond, V. R. and Hanssen, V., "The Burdet Formulation of the Perturbed Two-body Problem with Total Energy as an Element," *NASA-JSC-Internal Note*, Vol. 1, No. 73-FM-86 (JSC-O8004), 1973.

[45] Wakker, K. F., "Perturbing forces and perturbed satellite orbits," *Fundamentals of Astrodynamics*, chap. 20, Institutional Repository Delft University of Technology, 2015, pp. 527–554.

[46] Tapley, B. D., Schutz, B. E., and Born, G. H., "Observations," *Statistical Orbit Determination*, chap. 3, Elsevier, 2004, pp. 93–158.

[47] Geul, J., Mooij, E., and Noomen, R., "TLE Uncertainty Estimation using Robust Weighted Differencing," *Advances in Space Research*, Vol. 59, No. 10, 2017, pp. 2522–2535, doi: 10.1016/j.asr.2017.02.038.

[48] Vallado, D. A., "Special perturbation techniques," *Fundamentals of Astrodynamics and Applications*, chap. 8, Microcosm Press, 3rd ed., 2007, pp. 491–566.

[49] Picone, J. M., Hedin, A. E., Drob, D. P., and Aikin, A. C., "NRLMSISE-00 Empirical Model of the Atmosphere: Statistical Comparisons and Scientific Issues," *Journal of Geophysical Research*, Vol. 107, No. A12, 2002, pp. 1468–1483, doi: 10.1029/2002JA009430.

[50] Geul, J., Mooij, E., and Noomen, R., "Analysis of Uncertainties and Modeling in Short-Term Reentry Predictions," *Journal of Guidance, Control, and Dynamics*, Vol. 41, No. 6, 2018, pp. 1276–1289, doi: 10.2514/1.G003258.

[51] Stiefel, E. and Scheifele, G., "Typical perturbations," *Linear and Regular Celestial Mechanics*, chap. 6, Springer-Verlag, 1971, pp. 100–126.

[52] Montenbruck, O. and Gill, E., "Force Model," *Satellite orbits: models, methods and applications*, chap. 3, Springer Science & Business Media, 2012, pp. 53–113.

[53] Bergsma, M. and Mooij, E., "Application of Taylor-Series Integration to Reentry Problems with Wind," *Journal of Guidance, Control, and Dynamics*, 2016, pp. 2324–2335, doi: 10.2514/1.G000378.